AGU PUBLICATIONS

JGR

Journal of Geophysical Research: Space Physics

RESEARCH ARTICLE

10.1002/2017JA024578

Ion Heating in the Martian Ionosphere

C. M. Fowler[1], R. E. Ergun[1], L. Andersson[1], W. K. Peterson[1], T. Hara[2], J. Mcfadden[2], J. Espley[3], J. Halekas[4], D. L. Mitchell[2], C. Mazelle[5], and B. M. Jakosky[1]

[1]Laboratory for Atmospheric and Space Physics, University of Colorado Boulder, Boulder, CO, USA, [2]Space Sciences Laboratory, University of California, Berkeley, CA, USA, [3]NASA Goddard Space Flight Center, Greenbelt, MD, USA, [4]Department of Physics And Astronomy, University Of Iowa, Iowa City, IA, USA, [5]IRAP, University of Toulouse, CNRS, UPS, CNESS, Toulouse, France

Key Points:
- Energetic ions of up to a few hundred eV are observed in the Martian ionosphere
- Ion velocity distributions show ion conics, suggesting ions have been heated and experienced a magnetic mirror force
- Heating events occur primarily on the dayside, suggesting that the Mars-solar wind interaction influences the occurrence of such events

Correspondence to:
C. M. Fowler,
christopher.fowler@lasp.colorado.edu

Citation:
Fowler, C. M., Ergun, R. E., Andersson, L., Peterson, W. K., Hara, T., Mcfadden, J., … Jakosky, B. M. (2017). Ion heating in the Martian ionosphere. *Journal of Geophysical Research: Space Physics*, *122*. https://doi.org/10.1002/2017JA024578

Received 11 JUL 2017
Accepted 22 SEP 2017
Accepted article online 26 SEP 2017

Abstract Energetic O^+ and O_2^+ ions with energies of up to a few hundred eV are observed in the Martian ionosphere. Corresponding ion velocity distributions show ion conics, suggesting that the observed ion populations have been heated perpendicular to the local magnetic field before experiencing a magnetic mirror force. Magnetic field observations support these interpretations: wave power at the local O^+ and O_2^+ gyrofrequencies in the spacecraft frame is observed coincident with the energetic ions, within an apparent magnetic field bottle-like topology. Analysis of the observed ion conics leads to estimates of ion temperatures of 10–30 eV. We suggest that the ion populations are initially heated perpendicular to the local magnetic field by wave power propagating inward from the Mars-solar wind interaction. The local magnetic field "balloons out" in response to these enhanced ion temperatures and pressures. The resultant magnetic field topology is bottle like; the transversely heated ions would subsequently experience a magnetic mirror force in the converging field regions, agreeing with the reported observations. Such strong heating events that significantly increase the ion temperature and pressure, thereby decreasing the net magnetic field, are rare and seem to occur under specific interplanetary magnetic field orientations. Events were observed to span the upper exobase region and just above, a region characterized by significant ion densities in an increasingly collisionless domain. Ion heating in this region has the potential to drive significant ion outflows, thus contributing to atmospheric loss from the planet.

1. Introduction

The climate of Mars is known to have changed dramatically over the course of the planet's history. Many studies have shown that Mars was once a wetter planet, where liquid water was present on the surface and the atmosphere was thicker than its present-day counterpart (e.g., see the review by Jakosky & Phillips, 2001). Atmospheric loss to space is thought to have played a major role in this evolution, whereby energized neutral and charged particles escaped the gravitational potential of the planet and were lost to space (e.g., Chassefiere & Leblanc, 2004).

The acceleration and heating of ionospheric ions by various electro-magnetic and -static wave modes is one such mechanism to provide ions with sufficient energy such that they may escape the gravitational potential of a planet. Ion heating is observed in the terrestrial auroral region and has been the subject of extensive study. Wave-particle interactions can, for example, accelerate ions perpendicular to the local magnetic field, providing substantial energy to the bulk ion population (e.g., Temerin, 1986; Temerin & Roth, 1986). A variety of wave modes have been observed to heat ionospheric ions in the terrestrial auroral region, for example, Ungstrup et al. (1979), Chang and Coppi (1981), Sharp et al. (1983), Retterer et al. (1986), Chang et al. (1986), André et al. (1988), Vago et al. (1992), and Norqvist et al. (1998).

Within a converging magnetic field topology, such as the terrestrial auroral region, transversely heated ions are subject to the magnetic mirror force. Ions traveling into the converging magnetic field will lose velocity parallel to the magnetic field as they prepare to mirror. Ions traveling in the opposite direction, out of the converging field, will gain velocity parallel to the magnetic field, and at Earth such ions can be accelerated out of the ionosphere along the diverging magnetic field. This acceleration produces ion outflows that can lead to ion loss from the terrestrial ionosphere (e.g., Chaston et al., 2006; Knudsen et al., 1994; Mei et al., 2017;

Miyake et al., 1993, 1996; Pollock et al., 1990; Strangeway et al., 2005). A review of ion energization processes in the terrestrial magnetosphere can be found in André and Yau (1997), for example.

The much smaller mass of Mars means that the escape velocity for ionospheric (and neutral) species is much lower than at Earth; the escape energy of O^+ is ~2 eV at Mars, compared to ~10 eV at Earth, for example. Energization mechanisms thus need only to weakly energize ionospheric particles at Mars, relative to their terrestrial counterparts, in order to achieve escape energy. The location of this energization is important; ions heated well below the exobase (the exobase is located at about 180–200 km at Mars) will collide frequently with the neutral atmosphere and thermalize long before escaping. On the other hand, ion neutral collisions are rare well above the exobase. Ionospheric densities tend to be small (particularly above altitudes of ~400–500 km), and significant ion outflow rates cannot be achieved when heating occurs at these high altitudes. Ions observed at even greater altitudes are likely to already be escaping the planet, and additional heating will not increase the total outflow. Thus, the most important region for ionospheric heating and the driving of ion outflows at Mars, with regard to atmospheric escape to space, is located at altitudes just above and including the topside of the exobase (~190 to ~300–350 km).

Prior to the arrival of the Mars Atmosphere and Volatile EvolutioN (MAVEN) mission at Mars, energetic ions were observed within the planetary magnetosphere by the Phobos 2 spacecraft and within the ionosphere by the Mars EXpress (MEX) spacecraft. These ions were interpreted as heated ions (Lundin et al., 1989, 2004, 1990, 1989). Phobos 2 had a relatively high periapsis of ~900 km that did not sample the ionosphere, and MEX does not carry a magnetometer. It has thus not been possible to evaluate the importance of the magnetic field topology for these events and to determine the specific energization mechanisms of these ions.

This paper presents observations made by the MAVEN mission that strongly support these earlier interpretations of Phobos 2 and MEX data. MAVEN carries a complete plasma package and makes measurements all the way below the exobase to ~150 km on a regular basis. This paper demonstrates for the first time that ion conics exist within the Martian ionosphere and that the large ion temperatures observed can influence the surrounding plasma environment. The remainder of this paper is as follows: the data used are described in section 2; an example of an ion heating event observed in the Martian ionosphere is presented in section 3, with an accompanying discussion in section 3.5. The results of a statistical search for similar heating events are shown in section 4, with an accompanying discussion in section 4.2. Final conclusions are presented in section 5.

2. Instrumentation

The MAVEN mission entered Mars orbit on 22 September 2014; the spacecraft is in a 4.5 h elliptical orbit with a typical periapsis altitude of around 150 km (Jakosky et al., 2015). This study utilizes data from the Suprathermal and Thermal Ion Composition (STATIC, McFadden et al., 2015), Magnetometer (MAG, Connerney et al., 2015), Langmuir Probe and Waves (LPW, Andersson et al., 2015), and Solar Wind Electron Analyzer (SWEA, Mitchell et al., 2016) instruments.

STATIC is an electrostatic top hat analyzer that uses time of flight to determine ion mass. Electrostatic deflectors give the instrument a 360° × 90° field of view, and it is able to measure energies down to below 1 eV up to 30 keV and ion masses between 1 and 44 atomic mass units. STATIC has a measurement cadence of 4 s at periapsis for the data presented in this study. Science quality ion energy and ion mass spectra are available from the NASA Planetary Data System (PDS). Ion velocity distributions with respect to the local magnetic field are generated on ground using publicly available software provided by the STATIC instrument team.

MAG consists of two fluxgate magnetometers that each measure the vector magnetic field at a rate of 32 Hz. The two magnetometers provide hardware redundancy and allow for the calibration and correction for minor spacecraft-generated magnetic fields (Connerney, Espley, DiBraccio et al., 2015). Magnetic fields of up to 65,536 nT in strength can be measured, to an accuracy better than 0.05%. The 3-D magnetic field vector measured at 32 Hz is available from the NASA PDS. Magnetic field power spectra are generated on ground by performing a wavelet transform on the magnitude of the magnetic field vector, based on the process outlined in Torrence and Compo (1998).

LPW consists of two ~7 m booms separated by an angular distance of ~110°. Electric field power spectra, and electron densities and temperatures, are measured at a cadence of 4 s, for the data presented here. Electric field power spectra are obtained between frequencies of 2 Hz up to about 2 MHz. Electron densities and

temperatures are derived from analysis of I–V characteristics as described by Ergun et al. (2015). The instrument is designed to measure the cold, thermal electron population within the Martian ionosphere and as such can measure densities above ~20 cm^{-3} and temperatures between about 500 K and 20,000 K. All LPW data products presented in this study are available as science quality products from the NASA PDS.

SWEA is a hemispherical electrostatic analyzer that measures electron fluxes from 3 eV up to 5 keV. It has a 360° × 120° field of view provided by electrostatic deflectors and a time resolution of 2 s. SWEA has an energy resolution of 17% (ΔE/E) and is able to perform onboard real-time pitch angle mapping. Science quality electron energy spectra are available from the NASA PDS. Electron pitch angle distributions are produced on ground using publicly available software provided by the SWEA team.

Upstream solar wind conditions are available by request from Jasper Halekas (the primary investigator of the Solar Wind Ion Analyzer (SWIA, Halekas et al., 2015, instrument). The method used to calculate the upstream solar wind conditions used in this study is described in Halekas et al. (2017).

3. Event Study

3.1. Time Series Observations

Time series plasma observations of energetic ions in the Martian ionosphere are presented in Figure 1. Figures 1a and 1b show the omnidirectional ion energy and ion mass and spectra, respectively, measured by the STATIC instrument. Figure 1a has not been corrected for the spacecraft potential, and the spacecraft potential, as measured by STATIC, is overplotted as the black line. The black line is drawn against the *y* axis log scale of the panel. Figures 1c and 1d show the local electron density and electron temperature, respectively, measured by LPW. Figure 1e shows local magnetic field information: the black line shows the magnitude of magnetic field, measured by MAG, and the red line shows the magnitude of the modeled local crustal magnetic field (Morschhauser et al., 2014). The horizontal line marks a field strength of 34 nT, and this is discussed in section 3.5. The perpendicular variations in the local magnetic field are shown in Figure 1f; these are defined with respect to the spacecraft velocity, $\vec{\mathbf{V}}$: the quantity $\vec{\mathbf{B}}_\mathbf{0}$ is first obtained by smoothing the full-resolution 3-D magnetic field vector $\vec{\mathbf{B}}$ (not shown here) over a 16 s window. The perpendicular direction $\vec{\mathbf{B}}_\mathbf{1}$ is defined as the cross product $\vec{\mathbf{B}}_\mathbf{0} \times \vec{\mathbf{V}}$. The perpendicular direction $\vec{\mathbf{B}}_\mathbf{2}$ is defined as $(\vec{\mathbf{B}}_\mathbf{0} \times \vec{\mathbf{V}}) \times \vec{\mathbf{B}}_\mathbf{0}$. The magnitudes of $\vec{\mathbf{B}}_\mathbf{1}$ and $\vec{\mathbf{B}}^\mathbf{2}$ are obtained by calculating the dot product between the unit vector of $\vec{\mathbf{B}}_\mathbf{1}$ and $\vec{\mathbf{B}}_\mathbf{2}$ with $\vec{\mathbf{B}}$.

Absolute magnetic field wave power is shown in Figure 1g; the three lines from high to low frequency mark the local proton, O^+, and O_2^+ gyrofrequencies, respectively. The weak, roughly horizontal feature observed in the power spectrum at about 2–3 Hz is due to the spacecraft reaction wheels (Connerney, Espley, DiBraccio et al., 2015). One-dimensional electric field wave power is shown in Figure 1h. The omnidirectional superthermal electron energy spectrum, measured by SWEA, is shown in Figure 1i, with the corresponding electron pitch angle distribution for energies between 100 and 200 eV shown in Figure 1j. Figure 1k shows magnetic topology information: the black line shows the angle between the local magnetic field vector and the local vertical direction (angles <90° show upward pointing field; angles >90° show downward pointing field); the red line shows the angle between the local magnetic field vector and the spacecraft velocity vector (angles <90° show field-aligned travel; angles >90° show antiparallel travel along the local field). The spacecraft position, solar zenith angle, and altitude are shown as text below Figure 1k. Position is in the Mars Solar Orbital (MSO) frame, where *X* points along the planet-Sun line, Sunward; *Y* points opposite to Mars's orbital motion about the Sun; and *Z* completes the right-handed system. Gray colors in the spectrograms mark counts/energy fluxes that are below the color bar lower threshold.

For this periapsis, the spacecraft is located in the Southern Hemisphere, traveling in a northward direction on the dayside of the planet. Energetic ions are observed between the two solid vertical lines (12:17:44 and 12:22:56 UTC), identified by the substantial increase in energy flux above 10 eV in Figure 1a (this time period is also referred to as the "event" in this paper). The dashed vertical lines are discussed in section 3.3. Ion temperatures in the lower Martian ionosphere are typically below 0.1 eV (~1,000 K) (e.g., Hanson et al., 1977), and these energetic ions have thus been strongly energized. A corresponding ionospheric density depletion of almost an order of magnitude is observed in Figure 1c, and the electron temperature also increases by a factor of ~2–3. The ion temperature is estimated to be 10–30 eV during the event, as will be discussed in section 3.4. The total magnetic field strength decreases by about 30 nT when energetic ions are observed (Figure 1e). Wave power at the local O^+ and O_2^+ gyrofrequencies (in the spacecraft frame) is observed coincident with the

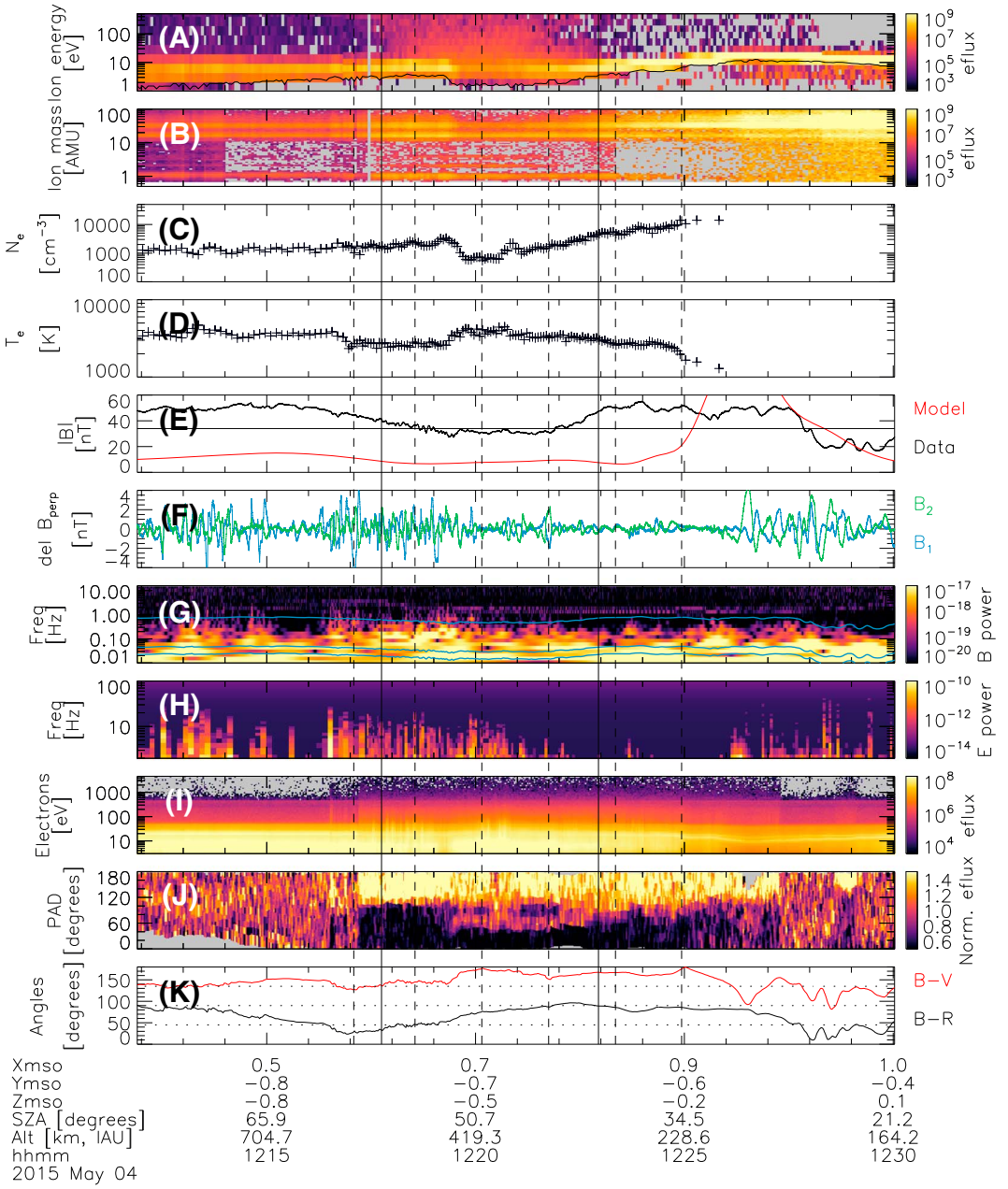

Figure 1. Time series plasma data of a single heating event, marked by the black solid vertical lines. (a) Ion energy (black line is spacecraft potential); (b) ion mass; (c) electron density; (d) electron temperature; (e) magnitude of magnetic field strength (black), crustal magnetic field model (red); (f) variations in magnetic field perpendicular to the field vector; (g) magnetic field power spectra; (h) 1-D electric field power spectra; (i) superthermal electron energy; (j) superthermal electron pitch angle distribution, for energies 100–200 eV; (k) angle between magnetic field and local zenith (black), angle between magnetic field and spacecraft velocity vector (red). Eflux has units of eV (eV cm^2 s sr)$^{-1}$; E power of $V^2m^{-2}Hz^{-1}$; B power of T^2Hz^{-1}.

energetic ions, particularly between about 12:18:30–12:20:00 UTC. Such waves are also clear in the magnitude of the magnetic field strength (Figure 1e) and the perpendicular components of the field (Figure 1f). Perpendicular wave amplitudes of around 4 nT (approaching 10% of the overall field strength) peak to peak are observed. Significant electric field wave power (which is also correlated with enhancements in magnetic field wave power below about 1 Hz) is also observed outside of the marked event, particularly between about 12:12 and 12:15 UTC (Figure 1h). These waves do not appear to be associated with any obvious ion heating but may provide electron heating as has been reported by Fowler et al. (2017). The solid black line in Figure 1k

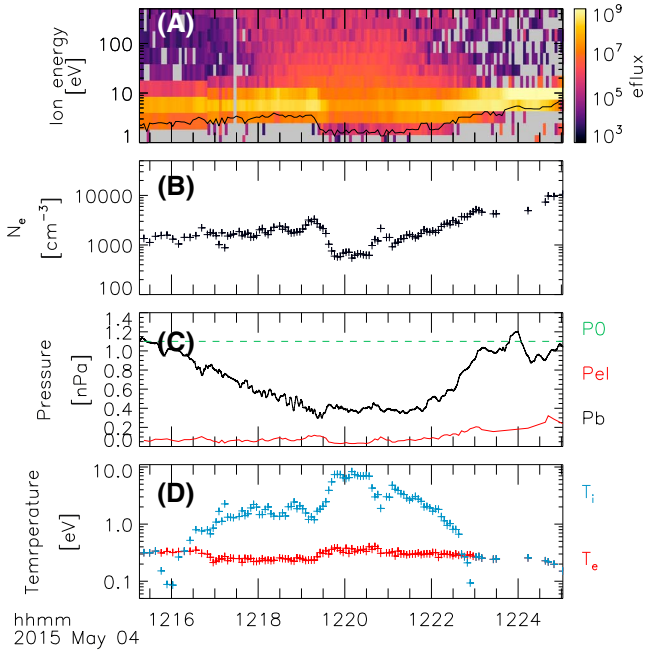

Figure 2. Estimates of ion temperature within the heating event. (a) Ion energy; (b) electron density; (c) magnetic pressure (black, calculated from data), electron pressure (red, calculated from data), and total pressure (green dashed line, assumed constant and equal to the sum of the magnetic, electron and ion pressures); (d) electron temperature (red), estimated ion temperature needed to conserve total pressure (blue).

shows that the magnetic field makes an angle of about 60°–70° to the local zenith at the start of the event (12:17 UTC) and is pointing upward (angle <90°). The field rotates to horizontal by about 12:20 UTC, where it remains for the remainder of the event. Electrons with pitch angles greater than 90° (Figure 1j) for the first half of the event are thus traveling downward, that is, toward the planet. Just after 12:17 UTC a wide beam of precipitating electrons with pitch angles greater than ~120° is observed in Figure 1j traveling into the ionosphere; analysis of individual spectra from Figure 1i (not shown here) confirms that these electrons are of solar wind origin. A second population is observed at pitch angles close to 90°, but upward traveling, between about 12:19:30 and 12:22:30 UTC. These observations suggest that solar wind electrons are precipitating into the ionosphere; localized heating of the thermal electron population occurs (marked by the increase in electron temperature in Figure 1d), and a small fraction of the precipitating electron population is reflected back up the field line.

3.2. Estimates of Ion Temperatures

For the remainder of this paper, the term ion temperature refers to the ion temperature perpendicular to the local magnetic field. Ion temperature for cold ionospheric plasma is difficult to reliably calculate in an automated fashion due to ongoing calibration of STATIC data at energies below about 5 eV (J. McFadden, private communication, 2017), but estimates can be obtained using two independent methods. The simplest is to assume quasi-neutrality of the plasma and to assume that the total pressure is constant over the heating region and is equal to the sum of the magnetic, electron, and ion pressures. The resulting ion temperatures needed to preserve constant pressure across the heating event are shown in Figure 2; Figures 2a and 2b show the ion energy spectra and electron density, respectively, as shown in Figure 1. Figure 2c shows various pressures: the red line shows electron pressure, calculated from measured values of electron density and temperature. The black line shows magnetic pressure, calculated from the measured magnetic field strength. The green dashed line shows the (assumed constant) total pressure, which is assumed equal to the sum of the magnetic, electron, and ion pressures, at the edge of the heating event (marked by the solid vertical lines in Figure 1; ion temperatures were assumed to be equal to the electron temperature at the edge of the heating event, where the magnetic pressure dominates).

Magnetic pressure dominates over the electron pressure outside of the heating event and is still a factor of at least ~5 greater when energetic ions are observed (Figure 2c). Figure 2d shows measured electron temperatures in red. The estimated ion temperatures required to maintain constant total pressure across the heating event, given the observed magnetic and electron pressures, are shown in blue. Ion temperatures of around 10 eV are required at the center of the event; the characteristic ion energies shown in Figure 2a suggest that these are realistic temperatures. We note that the assumption of constant pressure across the heating event is somewhat arbitrary; the analysis deals with ion temperatures perpendicular to the local magnetic field but assumes that pressure is constant along (or parallel to) the local magnetic field. Multiple spacecraft measurements, or modeling of the event, are required to improve this assumption. Ion temperatures can also be derived through manual analysis of ion velocity distributions, and this method is discussed in section 3.3.

3.3. Ion Velocity Distributions

Ion velocity distributions relative to the local magnetic field from the event shown in Figure 1 are shown in Figure 3. Figures 3a–3f show data for O^+; Figures 3g–3l show data for O_2^+ (these are the primary ion species at these altitudes in the dayside ionosphere, e.g., Benna et al., 2015). The horizontal and vertical axes show ion velocity parallel and perpendicular to the local magnetic field, respectively, where positive horizontal direction is along the field. Each velocity distribution is an integration across 4 s (the time it takes the STATIC instrument to make a full distribution measurement) and assumes ion gyrotropy. Time runs in ascending order from top to bottom in the figure. Due to telemetry restrictions, only a limited number of ion distributions can be sent to ground; a single distribution is shown in each panel, obtained within the time ranges shown in

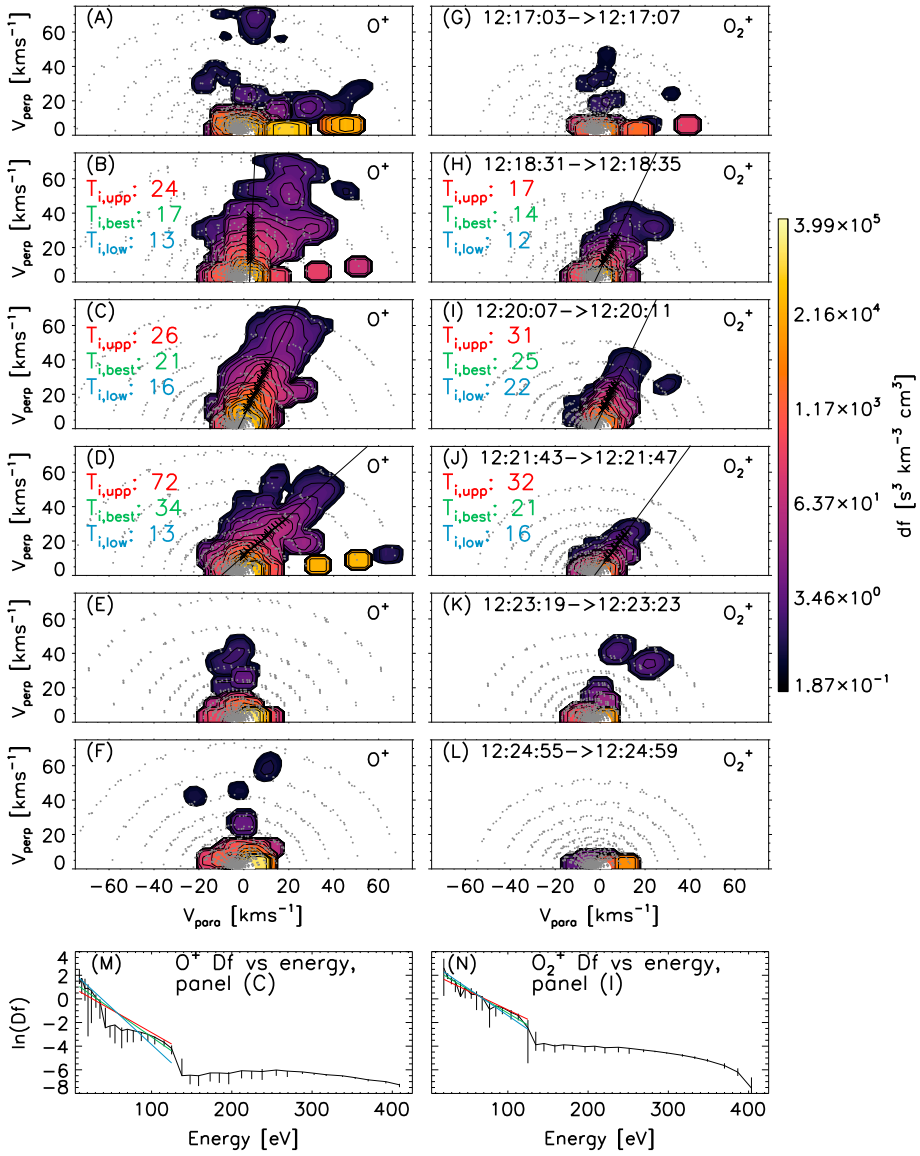

Figure 3. Ion velocity distributions from within the heating event. The time of each event is marked by the dashed vertical lines in Figure 1. (a–f) O^+. (g–l) O_2^+. (m, n) Example fits along the black lines in Figures 3c and 3i, respectively, used to derive ion temperatures. Best fit, upper, and lower, ion temperature estimates are shown in Figures 3b–3d and 3h–3j, in units of eV. See main text for more detail on the fitting method.

the right-hand column of panels. The midpoint in measurement time of each of the five ion distributions is marked by the dashed vertical lines in Figure 1. Gray dots in Figure 3 mark measurement points in velocity space; the contour plots show the ion distribution function interpolated to a regular grid that has horizontal and vertical resolutions of just over 1 km s^{-1}. Each distribution has been corrected for spacecraft velocity and potential. The black straight lines and black crosses in Figures 3b–3d and 3h–3j, along with Figures 3m and 3n, are discussed in section 3.4.

Ion distributions in the "undisturbed" ionosphere (Figures 3e and 3f) show O^+ populations with low temperatures. There is some evidence of heating perpendicular to the magnetic field, but the bulk of the population is cold. Progressing backward in time (upward in altitude), 3d, 3c, and 3b are distributions measured when energetic ions where observed, and the O^+ populations possess large velocities perpendicular to the local magnetic field. These ions also possess velocities parallel to the local magnetic field, and the distributions are known as ion conics (e.g., André and Yau, 1997). These ion populations are traveling in a positive direction along the magnetic field, which is pointed slightly upward for these times (Figure 1k). The distribution

shown in Figure 3a was observed outside of the heating event; the population possesses smaller perpendicular velocities to those in Figures 3d, 3c and 3b but is nonetheless still more disturbed than in Figures 3e and 3f. Similar behavior is observed for the O_2^+ populations.

3.4. Derivation of Ion Temperatures

If the ion populations observed within Figure 3 are assumed to be Maxwellian, the ion temperatures can be derived by fitting a straight line to the base 10 logarithm of the ion distribution function, as a function of ion energy, along the "ridge" of the ionconic. The ion temperature is the inverse of the gradient of this straight line (a similar method is outlined in more detail in, e.g., Sharp et al., 1983). Ion temperatures (T_i) were derived for the three velocity distributions observed within the heating event, for O^+ and O_2^+, corresponding to Figures 3b–3d and Figures 3h–3j. Ion temperatures were too cold to be accurately derived outside of the heating event for the distributions shown in the remaining panels. The black straight lines in Figures 3b–3d and 3h–3j mark where the ridge of each ion conic lies, determined by eye. T_i were derived from the interpolated data grid, using data points that lay closest to the straight black lines. The black crosses in each panel show the interpolated data points that were used to obtain each fit.

Figures 3m and 3n show example T_i fits from the distributions shown in Figures 3c and 3i. The horizontal axes show ion energy; the vertical axes show the base 10 logarithm of the ion distribution function. The error bars are estimated by plotting the maximum and minimum distribution function values found two interpolated grid points on either side of the primary measurement point. Due to ongoing STATIC instrument calibration, ions with velocity magnitudes less than 10 km s^{-1} were not included in the fitting. Ions with energy greater than 130 eV were also excluded from the fitting, as these energies appear to be attributed to a hot energetic tail population, rather than the bulk core population, as seen in Figures 3m and 3n.

The green lines in Figures 3m and 3n show the T_i best fits; the red and blue lines show estimates of the upper and lower temperature limits, respectively, based upon a 30% increase in the fit residual value, when T_i is increased and decreased from its best fit value. Similar plots were obtained for Figures 3b, 3d, 3h, and 3j and are not shown here because they essentially repeat Figures 3m and 3n. The T_i best fit values, and limits, are shown in the appropriate panels in Figure 3, in units of eV.

3.5. Interpretation and Discussion of the Event

It has long been thought that energy from the Mars-solar wind interaction is able to propagate into the Martian ionosphere and provide an ionospheric heating source. Evidence has been put fourth from studies of energy balance in the Martian ionosphere (Chen et al., 1978; Choi et al., 1998; Cui et al., 2015; Matta et al., 2014), analysis of the magnetic wave environment at Mars (Ergun et al., 2006; Espley et al., 2004), and more recently, by MAVEN observations showing correlations between electric field wave power and electron temperatures in the upper ionosphere (Fowler et al., 2017). Such ionospheric heating as a result of the planet-solar wind interaction has been observed at Venus (Scarf et al., 1980; Taylor et al., 1979).

We suggest an overall heating process similar to that put forth by Ergun et al. (2006). Waves produced in the sheath as a result of the Mars-solar wind interaction propagate into the upper Martian ionosphere (Figure 4a). Such waves may initially form as compressional modes due to the compressional nature of the solar wind forcing, but mode conversion may produce a mixture of compressional and transverse modes in the ionosphere. Such mode conversion has been observed at the terrestrial magnetopause (Johnson et al., 2001), and predicted to occur across plasma boundaries of increasing Alfvén velocity (Lin et al., 2012). These downward propagating waves may at some point become resonant with local ion gyrofrequencies within the ionosphere; at such times, ions are efficiently energized perpendicular to the local magnetic field by any transverse wave modes present. Using Mars Global Surveyor data, Ergun et al. (2006) showed that such an energy transfer mechanism could produce significant O^+ ion outflows at Mars.

The measurements presented in Figure 1 show that magnetic wave power is present at the O^+ and O_2^+ local gyrofrequencies in the spacecraft frame during the first half of the event (Figures 3e and 3f). The observed waves are likely Doppler shifted due to the spacecraft motion through the ionosphere (e.g., Stasiewicz et al., 2000); assuming that wave information propagates at the local Alfvén speed (which is typically on the order of a few km s^{-1} in the Martian ionosphere), such shifts may be on the order of a few hertz here. Without a full 3-D electric field measurement the wave vector relative to the spacecraft motion cannot be conclusively determined, leading to uncertainty in the magnitude of this shift. Wave power observed close to the local

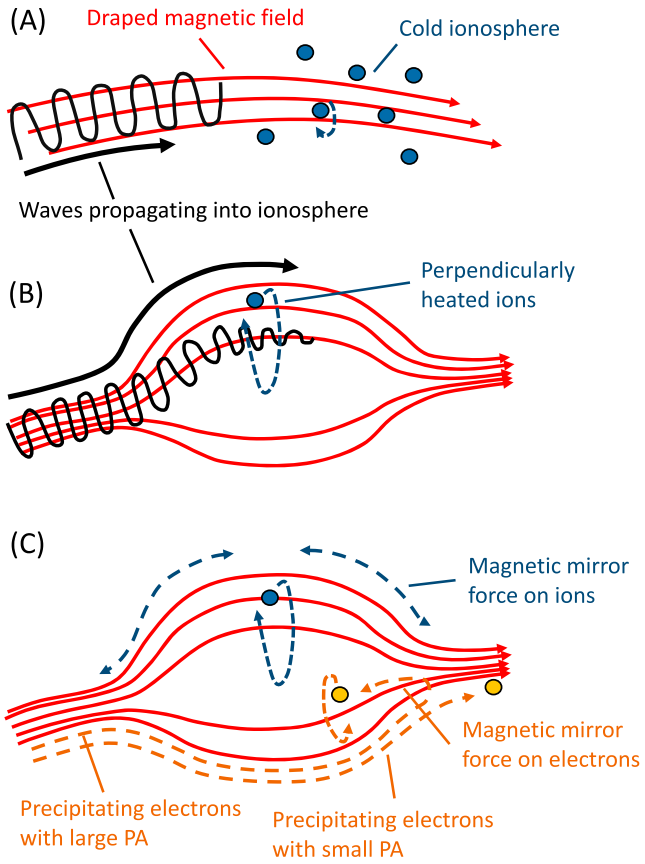

Figure 4. Cartoon depiction of the interpretation of the event shown in Figure 1 and described in section 3.5. Red solid lines depict local magnetic field lines; black solid lines depict waves propagating into the Martian ionosphere; solid blue and orange circles represent ionospheric ions, and precipitating electrons, respectively; dashed blue and orange lines depict the gyro and guiding center motion of ions and electrons, respectively.

ion gyrofrequencies is hence suggestive of ion cyclotron resonance but not conclusive. The lower hybrid frequency is on the order of a few hertz during the observed heating event; lower hybrid waves have been observed to cause significant ion heating in the terrestrial auroral region (e.g., Chang & Coppi, 1981); Vago et al., 1992); however, we do not believe that similar processes significantly contribute to the ion heating observed here because no lower hybrid cutoff is observed in Figure 1h.

Although only 1-D electric field wave power measurements are made by LPW, the orientation of the spacecraft when energetic ions were observed was such that an angle of about 30° – 40° was present between this 1-D electric field measurement and the local magnetic field vector. Thus, the electric field wave power shown in Figure 1h contains a component transverse to the local magnetic field that is able to provide perpendicular acceleration to the ions. LPW cannot measure frequencies below 2 Hz (typical O^+ gyrofrequencies within the Martian ionosphere are ~0.05 Hz), so resonance at the local O^+ and O_2^+ gyrofrequencies cannot be confirmed, but a DC component likely exists at lower frequencies, as observed in the magnetometer data.

The observed waves damp as they deposit energy into the ions, resulting in small wave amplitudes at the main heating region. This initially happens at low altitudes where the wave period is in resonance with the ion gyrofrequency, and enough ions exist to significantly dampen the wave. The ions are heated perpendicular to the local magnetic field, and if they exist in a magnetic gradient, they will mirror and start moving toward the region of lower strength magnetic field. If this region is toward the incident waves, then mirroring ions — now observable as ion conics — will enhance the ion thermal pressure. Assuming constant pressure, the enhanced ion thermal pressure will lead to decreased magnetic field strength and pressure, enhancing the gradient in magnetic field strength (we acknowledge that one must be careful here with causation and correlation — the observed enhanced ion temperatures correlate with decreases in magnetic pressure but which causes which can be debated). A change in magnetic field strength also changes the resonant frequency between the ions and incident waves.

This ion heating and erosion from the lower ionosphere is observed in Figure 3 as follows: The fairly unperturbed ionospheric ion distribution is seen in Figures 3f and 3e; no significant influence of a magnetic gradient is visible. Well-developed conics are observed in Figures 3d, 3c, and 3b; distributions at the lower energies of each distribution appear to follow similar pitch angles, and it is likely that no significant localized heating exists in these regions. We note, however, that due to the ongoing calibration at energies below 5 eV in STATIC data, the ability to discern between a "U"-shaped versus "V"-shaped distribution here is currently not conclusive. Were localized heating to exist, the observed conics would be U shaped (instead of the apparent observed V shaped) (André & Yau, 1997). Similar behavior is observed for O_2^+.

For the event presented here the ionosphere is initially eroded at lower altitudes and this erosion moves antiplanetward, creating the observed low density cavity (Figure 1c). The main heating and erosion edge are observed at ~20:19 in the electron density of Figure 1 and the reduction in wave power at the local O^+ and O_2^+ gyrofrequencies at the same time in Figure 1g. As a result of the decreasing ion density within the cavity, increasing amounts of wave power can pass through this initial heating region to the lower edge of the cavity, expanding it downward in altitude as well. The downward edge of the cavity is observed around ~20:23 UTC. The two black solid vertical lines in Figure 1 that mark the boundaries of the event will thus expand outward toward higher and lower altitudes over time.

Further evidence of a magnetic mirror effect is observed in the electron pitch angle distribution data (Figure 1j) by the population of electrons with pitch angles close to 90° but traveling upward along the magnetic field. The reflected electron population is not observed prior to 12:19:30 UTC; this time is coincident to when the angle between the MAVEN velocity vector and the local magnetic field vector changes by a significant amount.

The spacecraft is traveling at about ~145° to the local magnetic field before 12:19:30 UTC and is likely sampling flux tubes that do not possess reflected electrons at these earlier times.

Ions that are reflected between the magnetic mirror points may end up in a "magnetic mirror trap" situation. Ions are reflected at both sides of the density cavity due to the observed magnetic field gradient and become trapped within the magnetic bottle topology. Ion energy perpendicular to the local magnetic field thus increases substantially as a result of the ions passing through the heating region multiple times. The relatively small magnetic field strengths within the Martian ionosphere mean that as ions gain significant energy perpendicular to the local magnetic field, their gyro radii can become large (many tens or hundreds of kilometers) and their guiding center has an increasing chance of drifting to one that is not within the trap, allowing them to finally escape the heating region.

MAVEN flies antiparallel to the local magnetic field for the second half of the event, and ion conics are observed traveling upward toward the center of the magnetic bottle during such times. MAVEN flies at an angle to the magnetic field during the first half of the event and is likely sampling flux tubes that may not be connected to the bottle. The ion distributions in Figures 3a, 3b, 3g, and 3h show ions that are still traveling upward along the magnetic field, rather than being reflected back into the bottle, and these may represent ions that have escaped the bottle region.

A cartoon depiction of this interpretation is shown in Figure 4. Figure 4a depicts the undisturbed ionosphere where the magnetic field is in a draped configuration. As waves are assumed to propagate into the ionosphere (as per Ergun et al., 2006 for example), they heat ions perpendicular to the local magnetic field, Figure 4b. The resulting magnetic field topology, and the subsequent mirroring forces on the heated ionospheric ions, and precipitating electrons are depicted in Figure 4c. The lack of 3-D electric field measurements means that the wave propagation direction must be assumed here; statistical observations reported by Fowler et al. (2017) suggest that electric field wave power does propagate downward in the ionosphere, supporting the assumptions used here.

If the heated ion populations are assumed to possess pitch angles of 90° at the heating location within the magnetic bottle, a lower bound estimate of the magnetic field strength at this heating point can be made based on the observations presented in Figures 1 and 3. The conic fits in Figures 3c and 3i show that, in the approximate center of the proposed magnetic bottle, the O^+ and O_2^+ populations possess pitch angles relative to the local magnetic field of about 70°. Figure 1e shows that the corresponding magnetic field strength is about 30 nT. Using equation 3.62 in Cravens (2004), the magnetic field strength at the heating location is subsequently about 34 nT. If the heating is spread over a finite region of the bottle, this value is a lower limit because the field strength must be larger at the point where the heating starts. The black horizontal line in Figure 1e marks a field strength of 34 nT; the heated conics observed in Figures 3b–3d and 3h–3j lie within this lower bound and are thus consistent with the magnetic bottle interpretation.

An estimate of the size of the magnetic bottle region can be made based upon the observations presented in Figures 1 and 3, along with assuming that the bottle region is cylindrical in shape and aligned along the magnetic field. If the bottle is observed between the solid vertical lines in Figure 1, and MAVEN flies at an average angle of ~20° to the magnetic field throughout this region (Figure 1k) at a velocity of ~4 km s^{-1}, the bottle length is about 1,100 km. An estimate of the radius of this bottle is obtained by considering the observed ion motion within the bottle. Figure 3 shows that O^+ ions are observed at velocities up to at least ~75 km s^{-1} (this is the upper energy limit for the STATIC observation mode at periapsis). A lower limit of the bottle region radius can be determined by assuming that the observed ions are still trapped within the bottle region (and that if they were not trapped, they would not be present and thus not observed by the instrument). O^+ velocities of 75 km s^{-1} perpendicular to the local magnetic field correspond to gyroradii (and a bottle radius lower limit) of about 430 km. The bottle region size (particularly its length) appears to be a significant fraction of the planetary radius.

We include here a brief discussion of the limitations of single spacecraft in situ measurements and how these can limit our interpretations. The observed heating region is a three-dimensional structure, and the MAVEN spacecraft samples a single trajectory through it. It is thus difficult to determine the exact extent and geometry of the heating region. Single spacecraft measurements also present a challenge when interpreting apparent wave structure in the magnetic and electric field. MAVEN travels at about 4 km s^{-1} at periapsis, and there can be ambiguity as to whether signatures in the magnetic and electric field are due to waves or some other effect.

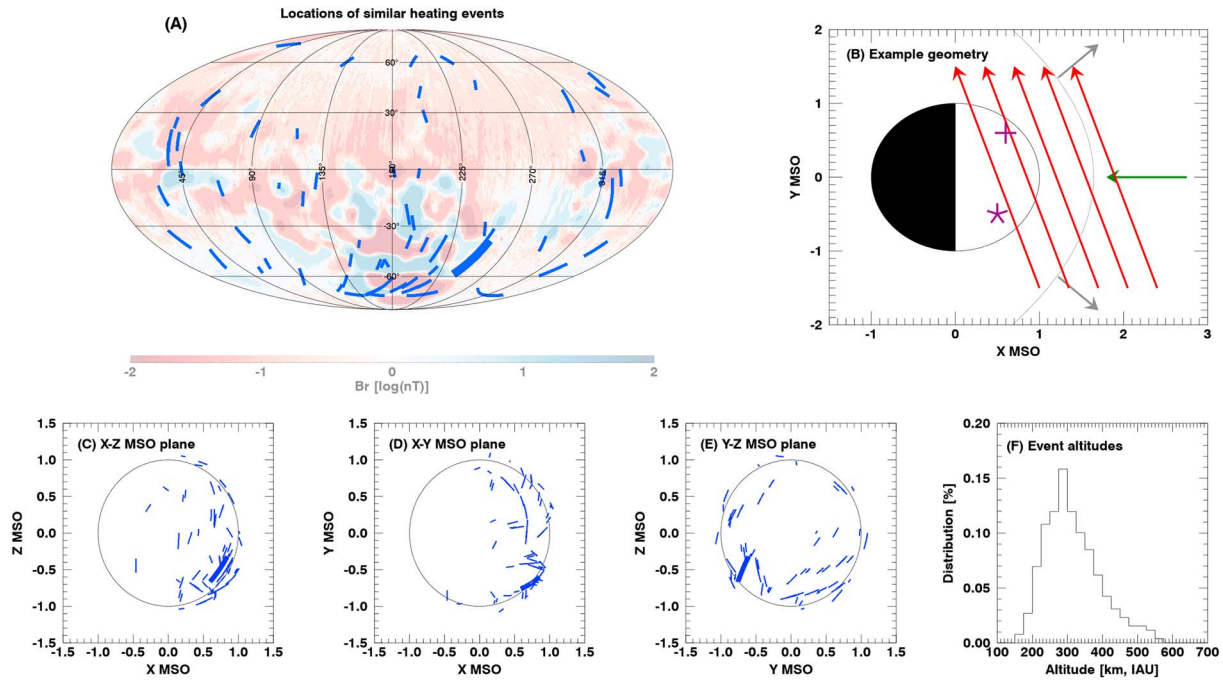

Figure 5. Statistical properties of the 65 similar heating events. (a) Location of each event, plotted as a blue line, over the crustal anomaly map, as a function of east longitude and latitude, in the Mollweide map projection. The thick blue line represents the event shown in Figure 1. (b) Cartoon example of upstream IMF geometry. (c–e) Locations of each event in the MSO *X-Z*, *X-Y*, and *Y-Z* planes, respectively. (f) Distribution of event altitudes.

A general rule of thumb has been to require at least three oscillations of the field to be present in order to classify the signature as a wave (e.g., Brain et al., 2002; Espley et al., 2004). As seen most easily in Figure 2c, on the order of ~5–10, oscillations are present between about 12:17:30 and 12:19:30 UTC, strongly supporting the existence of waves in the ionosphere. For the event studied here, the spacecraft velocity was about equal to the local Alfvén speed, and so Doppler shift effects make it difficult to determine the exact wave mode properties of the observed waves, which we have subsequently not attempted to estimate here.

4. Statistics of Similar Events

4.1. Method

A semi-automated search was carried out to identify similar heating events, where ions were significantly heated and a gradient in the magnetic field could be determined, over ~2.5 years of data, spanning 10 October 2014 to 31 March 2017. An automated routine identified time periods where enhanced ion energy flux was observed at energies greater than 10 eV in STATIC data, for altitudes below 600 km. Flagged events were then confirmed by eye, further, requiring a dip in the magnitude of the local magnetic field to be coincident in time with the observed energetic ions. Events were identified in a very conservative manner, flagging only the largest, most obvious events, similar to that shown in Figure 1. A total of 65 events were found. This semi-automated method was chosen because a fully automated ion temperature retrieval method for use with low energy (< 5 eV) STATIC data is currently unavailable. Such a routine is currently unavailable due to the calibration complexities associated with accounting for the evolution of surface properties within the STATIC instrument. The surface properties evolve over time due to exposure to atmospheric atomic oxygen; this evolution is most important at the lowest energies. Identifying such events is consequently difficult to do in a fully automated fashion, particularly within the Martian ionosphere which is highly variable in nature.

The locations that these heating events were observed at are shown as the blue lines in Figure 5, where each line represents a single event. The thick blue line marks the event shown in Figure 1. Figure 5a shows the locations as a function of east longitude and latitude in the Mollweide map projection, plotted over a map of the radial component of the magnetic crustal anomalies (Acuna et al., 1999), where B_r shows the log of radial field, positive upward. Figures 5c–5e show the event positions in the *X-Z*, *X-Y*, and *Y-Z* MSO planes. Figure 5f shows the altitude distribution of the 65 observed events. Figure 5b is discussed below.

Events are observed primarily on the dayside of the planet, with slightly more in the Southern Hemisphere where the largest crustal anomalies are situated (although events are also located outside of large crustal anomaly regions, see Figure 5a). The lack of events at the subsolar point may be due to limited sampling in this region as few MAVEN periapsis passes have yet reached such low solar zenith angles (below ~20°). The distribution of event altitudes (Figure 5f) peaks at about 300 km; very few events were observed below 200 km or above 500 km.

There was no obvious correlation between the upstream solar wind interplanetary magnetic field (IMF) orientation and the location and occurrence of observed heating events. An example cartoon depicting upstream IMF geometry in two dimensions is shown in Figure 5b; the green arrow represents the solar wind velocity flowing right to left, and the red lines represent the IMF orientation. The gray conic shows the empirical bow shock location as derived by Vignes et al. (2000); the two gray arrows show the local shock normal. Consider two example energetic ion events, on the dawnside and duskside of Mars, marked by the asterisk and cross, respectively. Under the IMF orientation shown, the IMF is quasi-parallel to the local shock normal for the asterisk event but quasi-perpendicular to the local shock normal for the cross event. The spacecraft cannot measure the upstream solar wind and the ionosphere simultaneously, and upstream conditions must thus be assumed constant for some length of time in order to represent the upstream conditions as the spacecraft samples the ionosphere. For the 65 flagged events analyzed here, the upstream conditions were assumed constant for 1, 1.5, 2, 3, and 4 h (for reference the MAVEN orbit period is about 4.5 h). The number of flagged events that subsequently had a "partner" upstream measurement were 4, 8, 14, 16, and 19, respectively (few partner measurements were available due to MAVENs orbit—for heating events located in the dayside ionosphere, MAVENs apoapsis is located in the tail and typically does not sample the undisturbed solar wind). Studies of discontinuities in the solar wind at 1 AU have shown that IMF rotations in the range of 30°–60° most commonly occur over time periods of about an hour (e.g., Burlaga, 1969), and so the assumption of constant IMF orientation for periods greater than 1 h is probably not appropriate; this method is, however, the best one can do with only a single spacecraft. The elliptical nature of MAVEN's orbit means that on any given orbit, the spacecraft does not observe the local shock and shock normal directly above heating events in the ionosphere. For simplicity, the local shock normal vector was hence assumed equal to the (3-D) radial vector of the spacecraft at the location that heating events were observed in the ionosphere. The angle between this quasi-shock normal vector and the (3-D) upstream IMF vector was calculated, and no obvious correlations were observed for quasi-parallel or perpendicular IMF orientations.

4.2. Discussion of Similar Event Statistics

The primarily dayside distributed locations of ion heating events suggest that the planet-solar wind interaction may be an important driver of the observed heating events. One may expect the upstream IMF to drive such events, but no obvious correlations were observed between heating event occurrence and upstream IMF orientation. This analysis required the assumption that IMF conditions were constant over periods of at least 1 h, because the MAVEN spacecraft cannot sample the upstream IMF orientation and ionosphere simultaneously. Short-term variability in IMF orientation may mask any correlations present, and this problem cannot be overcome with only a single spacecraft.

The clustering of heating events observed in regions of strong radial magnetic anomalies (Figure 5a) suggests that magnetic cusp regions may facilitate energy transfer into the ionosphere, providing localized heating in these regions. Heating events were also observed outside of strong radial magnetic anomalies (including the example shown in Figure 1), and further study is required to understand the importance of the crustal anomalies (if any) with regard to the observed ion heating events.

The altitude distribution of observed heating events (Figure 5f) shows that these events occur at altitudes just above the dayside Martian exobase, where collisions with the neutral atmosphere become infrequent and ionospheric densities are still significant (additional analysis showed that ionospheric densities during these events were typically 10^3–10^4 cm^{-3}). Thus, such events may drive strong ion outflows from the ionosphere, dependent on other factors such as the small- and large-scale magnetic topology (which is not a focus of this study, but has been studied previously, e.g., Brain et al., 2007; Lundin et al., 2011).

The small number of heating events observed in this study suggests that such large events are rare in the present-day Martian ionosphere—65 observed events (or periapsis passes) correspond to just over 1% of the total number of MAVEN orbits analyzed. Smaller heating events are likely present in the ionosphere but are more difficult to identify. An important next step is to determine whether these smaller events can be

reliably identified. The low escape energies at Mars mean that even mild heating would provide ample energization which could enhance ion outflow and escape. If smaller heating events are much more common in the ionosphere, they may be an important driver of ion outflow and atmospheric evolution at Mars.

Finally, it is important to discuss the limitations of the analysis method utilized in the statistical part of this study for flagging similar heating events. As has been stated, this study took a very conservative approach when flagging heating events. This arose because, as discussed in section 4.1, a reliable fully automated method to calculate cold (below a few eV) ionospheric temperatures from STATIC data is not yet available. Combined with the highly variable nature of the Martian ionosphere, this can make it difficult to discriminate between heating events and other ionospheric processes. Thus, less intense ion heating events are probably more common in the ionosphere, but the current identification method is unable to reliably identify heating events where ion temperatures are closer to a few eV or less. Further biases are likely present based on the spacecraft velocity vector through each observed heating region, relative to the size and shape of each heating region. Perpendicularly heated ions must also lie within the STATIC instrument field of view (FOV). Although the STATIC FOV is relatively large, there may be rare cases where such heated ion populations lie outside of the instrument FOV. We have not attempted to correct for any such biases in this study and have focused on reporting the basic characteristics of the observed events.

5. Conclusions

Energetic ions with energies of up to a few hundred eV have been observed in the Martian ionosphere. Ion conics are present in the corresponding ion velocity distributions, suggesting that populations have been heated perpendicular to the local magnetic field, before experiencing a magnetic mirror force. Observations of the local magnetic field support this theory; a magnetic bottle-like topology appears present during the periods in which energetic ions are observed. Analysis suggests that the ions are heated to temperatures of 10–30 eV; this large increase in ion temperature appears to cause the observed decrease in magnetic field strength (and corresponding magnetic pressure), resulting in the "ballooning out" of the local magnetic field, into a bottle-like topology. Such a topology would result in the heated ions being subject to a magnetic mirror force, explaining the observed ion conics. Electron pitch angle data show precipitating electrons also being reflected in the same region, supporting this theory.

Similar sized energetic ion events are rare in the current day Martian ionosphere—65 events were identified from 2.5 years of data. These events were observed to occur primarily on the dayside of Mars, between altitudes of ~200 and 400 km. This altitude range is located at altitudes just above and including the topside of the exobase, where ions are available to heat in significant densities but will not collide often with the neutral atmosphere. Such heated ions may thus produce significant ion outflows from the Martian ionosphere. The location of these observed events (dawn or dusk side of Mars) showed no obvious correlation with the upstream interplanetary magnetic field (IMF) orientation, although short-term variations in IMF direction may mask any correlations present. Events were observed primarily on the dayside of the planet suggesting that the Mars-solar wind interaction plays an important role in driving such events. Waves produced in the sheath due to the planet-solar wind interaction are postulated as a source of energy for these heating events. Such waves are suggested to propagate into the ionosphere, where they become resonant with the local ion gyrofrequency and cause significant heating, as suggested by Ergun et al. (2006).

Further investigation of these heating events is required to determine their importance for ion outflow and atmospheric evolution at Mars. This study analyzed only the strongest, most obvious heating events; smaller events are likely present and able to energize ionospheric constituents to the relatively low escape energies found at Mars.

Acknowledgments
Work at LASP and SSL was supported by NASA funding for the MAVEN project through the Mars Exploration Program under grant NNH10CC04C. Data used in this study are available on the NASA Planetary Data System, via https://pds.nasa.gov/. Wavelet software was provided by C. Torrence and G. Compo and is available at URL http://paos/colorado.edu/research/wavelets/.

References

Acuna, M., Connerney, J., Lin, R., Mitchell, D., Carlson, C., McFadden, J., … Cloutier, P. (1999). Global distribution of crustal magnetization discovered by the Mars Global Surveyor MAG/ER experiment. *Science*, *284*(5415), 790–793.

Andersson, L., Ergun, R., Delory, G., Eriksson, A., Westfall, J., Reed, H., … Meyers, D. (2015). The Langmuir probe and waves (LPW) instrument for MAVEN. *Space Science Reviews*, *195*(1–4), 173–198.

André, M., Koskinen, H., Matson, L., & Erlandson, R. (1988). Local transverse ion energization in and near the polar cusp. *Geophysical Research Letters*, *15*(1), 107–110.

André, M., & Yau, A. (1997). Theories and observations of ion energization and outflow in the high latitude magnetosphere. *Space Science Reviews*, *80*(1–2), 27–48.

Benna, M., Mahaffy, P., Grebowsky, J., Fox, J. L., Yelle, R. V., & Jakosky, B. M. (2015). First measurements of composition and dynamics of the Martian ionosphere by MAVEN's Neutral Gas and Ion Mass Spectrometer. *Geophysical Research Letters*, *42*, 8958–8965. https://doi.org/10.1002/2015GL066146

Brain, D., Bagenal, F., Acuna, M., Connerney, J., Crider, D., Mazelle, C., … Ness, N. (2002). Observations of low-frequency electromagnetic plasma waves upstream from the Martian shock. *Journal of Geophysical Research*, *107*(A6), SMP 9-1–SMP 9-11. https://doi.org/10.1029/2000JA000416

Brain, D., Lillis, R., Mitchell, D., Halekas, J., & Lin, R. (2007). Electron pitch angle distributions as indicators of magnetic field topology near Mars. *Journal of Geophysical Research*, *112*, A09201. https://doi.org/10.1029/2007JA012435

Burlaga, L. F. (1969). Directional discontinuities in the interplanetary magnetic field. *Solar Physics*, *7*(1), 54–71.

Chang, T., & Coppi, B. (1981). Lower hybrid acceleration and ion evolution in the suprauroral region. *Geophysical Research Letters*, *8*(12), 1253–1256. https://doi.org/10.1029/GL008i012p01253

Chang, T., Crew, G., Hershkowitz, N., Jasperse, J., Retterer, J., & Winningham, J. (1986). Transverse acceleration of oxygen ions by electromagnetic ion cyclotron resonance with broad band left-hand polarized waves. *Geophysical Research Letters*, *13*(7), 636–639.

Chassèfiere, E., & Leblanc, F. (2004). Mars atmospheric escape and evolution; interaction with the solar wind. *Planetary and Space Science*, *52*(11), 1039–1058.

Chaston, C., Génot, V., Bonnell, J., Carlson, C., McFadden, J., Ergun, R., … Hwang, K. (2006). Ionospheric erosion by Alfvén waves. *Journal of Geophysical Research*, *111*, A03206. https://doi.org/10.1029/2005JA011367

Chen, R., Cravens, T., & Nagy, A. (1978). The Martian ionosphere in light of the Viking observations. *Journal of Geophysical Research*, *83*(A8), 3871–3876. https://doi.org/10.1029/JA083iA08p03871

Choi, Y., Kim, J., Min, K., Nagy, A., & Oyama, K. (1998). Effect of the magnetic field on the energetics of Mars ionosphere. *Geophysical Research Letters*, *25*(14), 2753–2756.

Connerney, J., Espley, J., DiBraccio, G., Gruesbeck, J., Oliversen, R., Mitchell, D., … Jakosky, B. (2015). First results of the MAVEN magnetic field investigation. *Geophysical Research Letters*, *42*, 8819–8827. https://doi.org/10.1002/2015GL065366

Connerney, J. E. P., Espley, J., Lawton, P., Murphy, S., Odom, J., Oliversen, R., & Sheppard, D. (2015). The MAVEN magnetic field investigation. *Space Science Reviews*, *195*, 257–291. https://doi.org/10.1007/s11214-015-0169-4

Cravens, T. E. (2004). *Physics of Solar System Plasmas*. Cambridge, UK: Cambridge University Press.

Cui, J., Galand, M., Zhang, S., Vigren, E., & Zou, H. (2015). The electron thermal structure in the dayside Martian ionosphere implied by the MGS radio occultation data. *Journal of Geophysical Research: Planets*, *120*, 278–286. https://doi.org/10.1002/2014JE004726

Ergun, R. E., Andersson, L., Peterson, W. K., Brain, D., Delory, G. T., Mitchell, D. L., … Yau, A. W. (2006). Role of plasma waves in Mars' atmospheric loss. *Geophysical Research Letters*, *33*, L14103. https://doi.org/10.1029/2006GL025785

Ergun, R., Morooka, M., Andersson, L., Fowler, C., Delory, G., Andrews, D. J., … Jakosky, B. (2015). Dayside electron temperature and density profiles at Mars: First results from the MAVEN Langmuir probe and waves instrument. *Geophysical Research Letters*, *42*, 8846–8853. https://doi.org/10.1002/2015GL065280

Espley, J., Cloutier, P., Brain, D., Crider, D., & Acuña, M. (2004). Observations of low-frequency magnetic oscillations in the Martian magnetosheath, magnetic pileup region, and tail. *Journal of Geophysical Research*, *109*, L14103. https://doi.org/10.1029/2003JA010193

Fowler, C. M., Andersson, L., Peterson, W. K., Halekas, J., Nagy, A. F., Ergun, R. E., … Jakosky, B. M. (2017). Correlations between enhanced electron temperatures and electric field wave power in the Martian ionosphere. *Geophysical Research Letters*, *44*. https://doi.org/10.1002/2017GL073387

Halekas, J., Ruhunusiri, S., Harada, Y., Collinson, G., Mitchell, D., Mazelle, C., … Jakosky, B. M. (2017). Structure, dynamics, and seasonal variability of the mars-solar wind interaction: Maven solar wind ion analyzer in-flight performance and science results. *Journal of Geophysical Research: Space Physics*, *122*, 547–578. https://doi.org/10.1002/2016JA023167

Halekas, J., Taylor, E., Dalton, G., Johnson, G., Curtis, D., McFadden, J., … Jakosky, B. (2015). The solar wind ion analyzer for MAVEN. *Space Science Reviews*, *195*(1–4), 125–151.

Hanson, W., Sanatani, S., & Zuccaro, D. (1977). The Martian ionosphere as observed by the Viking retarding potential analyzers. *Journal of Geophysical Research*, *82*(28), 4351–4363. https://doi.org/10.1029/JS082i028p04351

Jakosky, B. M., Lin, R., Grebowsky, J., Luhmann, J., Mitchell, D., Beutelschies, G., … Zurek, R. (2015). The Mars atmosphere and volatile evolution (MAVEN) mission. *Space Science Reviews*, *195*(1–4), 3–48.

Jakosky, B. M., & Phillips, R. J. (2001). Mars' volatile and climate history. *Nature*, *412*(6843), 237–244.

Johnson, J. R., Cheng, C., & Song, P. (2001). Signatures of mode conversion and kinetic Alfvén waves at the magnetopause. *Geophysical Research Letters*, *28*(2), 227–230.

Knudsen, D., Whalen, B., Abe, T., & Yau, A. (1994). Temporal evolution and spatial dispersion of ion conics: Evidence for a polar cusp heating wall. *Solar System Plasmas in Space and Time*, 163–169. https://doi.org/10.1029/GM084p0163

Lin, Y., Johnson, J. R., & Wang, X. (2012). Three-dimensional mode conversion associated with kinetic Alfvén waves. *Physical Review Letters*, *109*(12), 125003.

Lundin, R., Barabash, S., Andersson, H., Holmstrom, M., Grigoriev, A., Yamauchi, M., … Bochsler, P. (2004). Solar wind-induced atmospheric erosion at Mars: First results from ASPERA-3 on Mars Express. *Science*, *305*(5692), 1933–1936.

Lundin, R., Barabash, S., Yamauchi, M., Nilsson, H., & Brain, D. (2011). On the relation between plasma escape and the Martian crustal magnetic field. *Geophysical Research Letters*, *38*, L02102. https://doi.org/10.1029/2010GL046019

Lundin, R., Zakharov, A., Pellinen, R., Barabasj, S., Borg, H., Dubinin, E., … Pissarenko, N. (1990). ASPERA/Phobos measurements of the ion outflow from the Martian ionosphere. *Geophysical Research Letters*, *17*(6), 873–876.

Lundin, R., Zakharov, A., Pellinen, R., Borg, H., Hultqvist, B., Pissarenko, N., … Koskinen, H. (1989). First measurements of the ionospheric plasma escape from Mars. *Nature*, *341*(6243), 609–612.

Matta, M., Galand, M., Moore, L., Mendillo, M., & Withers, P. (2014). Numerical simulations of ion and electron temperatures in the ionosphere of Mars: Multiple ions and diurnal variations. *Icarus*, *227*, 78–88.

McFadden, J., Kortmann, O., Curtis, D., Dalton, G., Johnson, G., Abiad, R., … Jakosky, B. (2015). MAVEN suprathermal and thermal ion compostion (STATIC) instrument. *Space Science Reviews*, *195*(1–4), 199–256.

Mei, L., Lotko, W., Varney, R. H., & Huba, J. D. (2017). Parametric study of density cavities caused by ion outflow in the topside ionosphere. *Journal of Atmospheric and Solar-Terrestrial Physics*, *156*, 37–49. https://doi.org/10.1016/j.jastp.2017.02.013

Mitchell, D., Mazelle, C., Sauvaud, J.-A., Thocaven, J.-J., Rouzaud, J., Fedorov, A., … Jakosky, B. M. (2016). The MAVEN solar wind electron analyzer. *Space Science Reviews*, *200*(1–4), 495–528.

Miyake, W., Mukai, T., & Kaya, N. (1993). On the evolution of ion conics along the field line from EXOS D observations. *Journal of Geophysical Research: Space Physics*, *98*(A7), 11,127–11,134.

Miyake, W., Mukai, T., & Kaya, N. (1996). On the origins of the upward shift of elevated (bimodal) ion conics in velocity space. *Journal of Geophysical Research: Space Physics*, *101*(A12), 26,961–26,969.

Morschhauser, A., Lesur, V., & Grott, M. (2014). A spherical harmonic model of the lithospheric magnetic field of Mars. *Journal of Geophysical Research: Planets*, *119*(6), 1162–1188. https://doi.org/10.1002/2013JE004555

Norqvist, P., André, M., & Tyrland, M. (1998). A statistical study of ion energization mechanisms in the auroral region. *Journal of Geophysical Research*, *103*(A10), 23,459–23,473.

Pollock, C., Chandler, M., Moore, T., Waite, J., Chappell, C., & Gurnett, D. (1990). A survey of upwelling ion event characteristics. *Journal of Geophysical Research*, *95*(A11), 18,969–18,980.

Retterer, J. M., Chang, T., & Jasperse, J. (1986). Ion acceleration by lower hybrid waves in the suprauroral region. *Journal of Geophysical Research*, *91*(A2), 1609–1618.

Scarf, F., Taylor, W., Russell, C., & Elphic, R. (1980). Pioneer Venus plasma wave observations: The solar wind-Venus interaction. *Journal of Geophysical Research*, *85*(A13), 7599–7612.

Sharp, R., Lennartsson, W., Peterson, W., & Ungstrup, E. (1983). The mass dependence of wave particle interactions as observed with the ISEE-1 energetic ion mass spectrometer. *Geophysical Research Letters*, *10*(8), 651–654.

Stasiewicz, K., Khotyaintsev, Y., Berthomier, M., & Wahlund, J.-E. (2000). Identification of widespread turbulence of dispersive Alfvén waves. *Geophysical Research Letters*, *27*(2), 173–176. https://doi.org/10.1029/1999GL010696

Strangeway, R., Ergun, R., Su, Y.-J., Carlson, C., & Elphic, R. (2005). Factors controlling ionospheric outflows as observed at intermediate altitudes. *Journal of Geophysical Research*, *110*, A03221. https://doi.org/10.1029/2004JA010829

Taylor, W., Scarf, F., Russell, C., & Brace, L. (1979). Absorption of whistler mode waves in the ionosphere of Venus. *Science*, *205*(4401), 112–114.

Temerin, M. (1986). Evidence for a large bulk ion conic heating region. *Geophysical Research Letters*, *13*(10), 1059–1062.

Temerin, M., & Roth, I. (1986). Ion heating by waves with frequencies below the ion gyrofrequency. *Geophysical Research Letters*, *13*(11), 1109–1112.

Torrence, C., & Compo, G. P. (1998). A practical guide to wavelet analysis. *Bulletin of the American Meteorological Society*, *79*(1), 61–78.

Ungstrup, E., Klumpar, D. M., & Heikkila, W. J. (1979). Heating of ions to superthermal energies in the topside ionosphere by electrostatic ion cyclotron waves. *Journal of Geophysical Research*, *84*(A8), 4289–4296.

Vago, J. L., Kintner, P., Chesney, S., Arnoldy, R., Lynch, K., Moore, T., & Pollock, C. (1992). Transverse ion acceleration by localized lower hybrid waves in the topside auroral ionosphere. *Journal of Geophysical Research*, *97*(A11), 16,935–16,957.

Vignes, D., Mazelle, C., Reme, H., Acuña, M., Connerney, J., Lin, R., … Ness, N. (2000). The solar wind interaction with Mars: Locations and shapes of the bow shock and the magnetic pile-up boundary from the observations of the MAG/ER experiment onboard Mars Global Surveyor. *Geophysical Reserach Letters*, *27*(1), 49–52. https://doi.org/10.1029/1999GL010703